An *in vivo* coil setup for AC magnetic field-mediated magnetic nanoparticle heating experiments

Arkadiusz Miaskowski, Preethiya Balakrishnan, Mahendran Subramanian, and Ondrej Hovorka

***Abstract*— *In vitro* and *in vivo* evaluation of magnetic nanoparticles in relation to magnetic fluid hyperthermia (MFH) treatment is an on-going quest. This current paper demonstrates the design, fabrication, and evaluation of an *in vivo* coil setup for real-time, whole body thermal imaging. Numerical calculations estimating the flux densities, and *in silico* analysis suggest that the proposed *in vivo* coil setup could be used for real-time thermal imaging during MFH experiments (within the limitations due to issues of penetration depth). Such *in silico* evaluations provide insights into the design of suitable AMF applicators for AC magnetic field-mediated *in vivo* MNP heating as demonstrated in this study.**

I. INTRODUCTION

Alternating magnetic field (AMF) mediated magnetic nanoparticle (MNP) heating has copious biomedical applications [1,2]. Non-contact temperature measurement technology, such as infra-red thermal camera and pyrometer require direct optical exposure [3,4]. This involves heat loss from the sample. Contamination is also possible when using the in-contact temperature measurement probes such as thermocouple and fibre optics.

Furthermore, metals are prone to radio frequency (RF) and electromagnetic (EM) interference [5-7]. MRI mediated non-contact temperature measurement is plausible and suitable, but, customisation, accessibility, ease of use and cost involved require consideration [8]. Herein, we built an *in vivo* coil setup embedded within a small animal bed, with water jacket and a viewing window, for real-time - whole thermal imaging during MFH experiments and analysed this setup using *in silico* techniques.

II. MATERIALS AND METHODS

A. Flux density simulation and calculation

The magnetic flux density (B) was simulated. This was done by the Sim 4 Life (ZMT Zurich Med Tech, Zurich) platform. The flux distribution was modelled in relation to an applied low-frequency magneto-quasi static (LF M-QS) algorithm utilising the finite element method (FEM) model.

*Research supported by nanoTherics Ltd. A. M. is with the Department of Applied Mathematics and Computer Science, University of Life Sciences, Lublin, Lublin, Poland (e-mail: arek.miaskowski@up.lublin.pl). P. B. is with the Faraday-Fleming Laboratory, Research and Development Department, London, United Kingdom (e-mail: preethiya.balakrishnan@gmail.com). M. S. is with the Department of Bioengineering and Department of Computing, Imperial College London, London, United Kingdom (Corresponding author e-mail: m.subramanian@imperial.ac.uk). And M.S. is currently supported by the EPSRC and Imperial College London [EP/N509486/1: 1979819]. O. H. is with the Faculty of Engineering and Physical Sciences, University of Southampton, Southampton, United Kingdom (e-mail: o.hovorka@soton.ac.uk).

Here, the coil wire was treated as a perfect electric conductor (PEC). The curved planar coil was modelled, includes: D_t = 6 mm, d_t = 4 mm, g_{cu} = 1.22 mm, N = 11, l = 1, SN = 4 mm, d_c = 5 mm, D_c = 60 mm, and C_i (internal curvature) = 90 mm. In this case, we presented the coil mathematically as an Archimedean spiral then transformed its planar geometry to circular geometry so that it would appear to lie on a plastic cylinder.

B. Curved planar coil fabrication

Hollow water-cooled coils were fabricated using 18 standard wire gauge (SWG) copper wire (Maplin, Stoke on Trent, UK) and silicon tube (Saint-Gobain, Coventry, UK) with dimensions 4 mm ID x 6 mm OD. A curved planar coil form was designed (PTC Creo 4.0, Staffordshire, UK) and precision engineered (3D printer – Flash forge, London, UK) for use in winding and preserving the geometry of the coil.

C. Single-domain magnetic power losses

In addition to the power losses due to the eddy current effect, a power dissipation from magnetic nanoparticles (MNPs) should be considered in parallel when dealing with MFH. When single-domain MNPs in the paramagnetic regime are exposed to an AMF with given parameters (H_{max}, f), the magnetisation lags behind the external field thus specific loss power can be express as

$$SLP_{LRT} = \int_0^{V_0} \pi\mu_0\chi'' H_{max}^2 f \rho V_M g(\mu,\sigma,V_M) dV \quad (1)$$

where ρ is the density of MNPs and $X^{''}$ is the average out-of-phase component of the susceptibility given by

$$\chi'' = \frac{\mu_0\mu}{3k_BT}\frac{2\pi f\tau}{(1+(2\pi f\tau)^2)} \quad (2)$$

where τ is the Neel-Brown relaxation time k_B is the Boltzmann constant, T is the temperature, μ is the magnetic moment of the magnetic particle defined as $\mu = M_S V_M$ where M_s stands for the saturation magnetisation and V_M stands for the magnetic volume of the nanoparticle ($\pi D_M^3/6$). Taking into account, the polydisperse character of MNPs expressed as the volume weighted distribution $g(\mu,\sigma,V_M)$ together with the Zeeman condition one can find a critical diameter/volume above which the MNPs will be blocked. In this case, specific loss power can be expressed as

$$SLP_{S-W} = 2\mu_0 M_s f \rho^{-1} \int_{V_0} H_c(V) g(\mu, \sigma, V_M) dV \quad (3)$$

where H_c is the coercively [11-13].

D. Eddy current effect

When human tissues are exposed to an alternating electromagnetic field, the eddy current effect is observed due to non-zero conductivity (σ) of the tissues, which ultimately leads to their heating [9]. In order to include a volumetric power density (P_{eddy}) produced by an eddy current (J_{eddy}) effect, a magneto-quasi static algorithm was applied [10]. P_{eddy} can be expressed as:

$$P_{eddy} = \frac{J_{eddy}^2}{\sigma} \quad (4)$$

Discussing the eddy or Foucault currents is essential due to their effects on different types of tissues when exposed to a time-varying magnetic field. The eddy current effect can lead to unwanted non-specific heating of healthy tissues, so must be considered in the applicator design.

E. In vivo numerical modelling

The thermal properties of the rat tissue model were calculated for *f* = 107 kHz using a 4-Cole-Cole approximation based on IT'IS database [15]. The following properties of magnetite were used: magnetic saturation 92.0 kA/m, the anisotropy constant 30 kJ/m3, the surfactant layer thickness 2.0 nm and the density 5180 kg/m3. Log-normal volume weighted particle distribution was assumed (median = 10.3 nm, standard deviation = 0.16). Volume weighted log-normal distribution was used for the MNPs. The spatial distribution of the MNPs in the tumour volume was considered homogenous, i.e. the volume of the ferrofluid and the volume of the tumour tissue were the same. The concentration of MNPs in the tumour was raised to 15 mg/ml in order to generate the desired temperature in the tumour area.

Table 1: *Biological and technical information concerning the rat model [16].*

Sex	Weight	Length (snout - vent)	Length (total)	Properties	Description	No. of slices	Slice separation for discretization
female	503 g	22.5 cm	38.5 cm	1 tumour	Sprague Dawley	738	1.052 mm

The MNP relaxation times were estimated using magnetic field dependent formulas. For Brownian relaxation, the viscosity of blood was used instead of water. When comparing MNPs suspended in a solution with MNPs suspended in the tumour tissue, the Neel relaxation time was the same. The biological and technical information concerning the rat model can be seen in Table 1. Various tissues were added in order to construct a life-like *in vivo* numerical model.

F. Pennes equation

In this case, the heat generation rate, the perfusion and the heat-transfer rate were made linearly dependent on the temperature ($aT + b$) to account for the strong temperature dependence due to bio-regulatory processes. Hence, the temperature distribution in the breast model was investigated using the modified bio-heat transfer equation formulated by [14]:

$$\rho c \frac{\partial T}{\partial t} = \nabla \cdot (\kappa \nabla T) + \rho_b c_b \omega (T_b - T) + P_{met} + P_{ext} \quad (5)$$

where ρ is the tissue density [kg/m], c is the tissue-specific heat [J/kg/C], ρ_b is the density of blood [kg/m3], c_b is blood specific heat [J/kg/C], κ is the tissue thermal conductivity [W/m/C]), ω is the perfusion rate [1/s], T_b is the arterial blood temperature [C], T is the local temperature [C], P_{met} is the metabolic heat source [W/m^3], and $P_{ext} = \rho_{MNP}(SLP_{LRT} + SLP_{S-W}) + P_{eddy}$ is the external heat due to eddy currents and the magnetic nanoparticles power losses [W/m^3]. The convection boundary condition (Robins type) was used:

$$\kappa \frac{\partial T}{\partial n} = h(T_{ext} - T) \quad (6)$$

where h is the heat transfer coefficient, and κ is the thermal conductivity. $T_{he\ text}$ stands for external air temperature. The same value is used as an initial boundary condition, $T\ (t = 0) = T_{ext}$.

III. Results and Discussion

In MFH, a low-cost thermal imaging technique has been successfully used for obtaining real-time *in vitro* and *in vivo* surface temperature measurements [17-19]. This is beneficial for heat dosimetry and clinical planning. It is possible to estimate the power dissipation from MNPs and intratumoral temperature increase based on the surface temperature measurements [20]. Furthermore, the technique is non-contact and covers a wide area, which is a significant advantage over point-measurement techniques [21]. Thus, an efficient applicator design that will enable the performance of *in vivo* AMF exposure and thermal imaging simultaneously is required.

This *in vivo* coil design was inspired by the shim coil used to adjust the homogeneity of a static magnetic field by changing the current flowing through it for high-resolution MRI. The curvature of the coil will depend upon the *in vivo* water jacket OD, and the geometry of the *in vivo* coil used for calculations is shown in fig.1a. The curved planar coil *in vivo* set up (the CAD model), and the flux density calculations can be seen in fig.1. Calculations revealed that the incident flux density is non-homogenous and failed to cover the whole of the animal model (Fig.1d). The flux density in the z-axis ranged up to $\mu_0 H$ = 31.42 mT (Fig.1c).

Magnetic hysteresis modelling is complex, and Linear Response Theory (LRT) for correlation with experimental data has been under scrutiny, since the characterization of bulk and microscopic properties (static and dynamic), such as intercore dipole interactions and differences in internal magnetic (intracore) structure, will affect the heating performance of the ferrofluids. Measurements limited to amplitudes lower than saturation usually fail to establish the nonlinearity of power loss [22] and stirring-mediated power loss due to aggregated nanoparticles in an aqueous suspension cannot be neglected [23]. However, in recent years, LRT has been evaluated and modified for magnetic hysteresis modelling considering the importance of the dispersity index and the nanoparticle anisotropy constant [24]. Furthermore, high nanoparticle concentrations were found to correlate with increasing chain length, and when the magnetic dipolar contribution was considered, a decrease in hyperthermia efficiency was demonstrated [25]. Moreover, the heat dissipation due to susceptibility loss is low and can be neglected, with hysteresis loss being the dominant mechanism based on the power loss measurements and calculations performed on the HyperMAG® particles (Liquids research, UK) [23] used in this study. Nonetheless, discrepancies with estimated parameters and theoretical predictions arising due to particle-particle interactions require normalisation. Besides, it must be acknowledged that an accurate prediction of SAR is difficult [26-28].

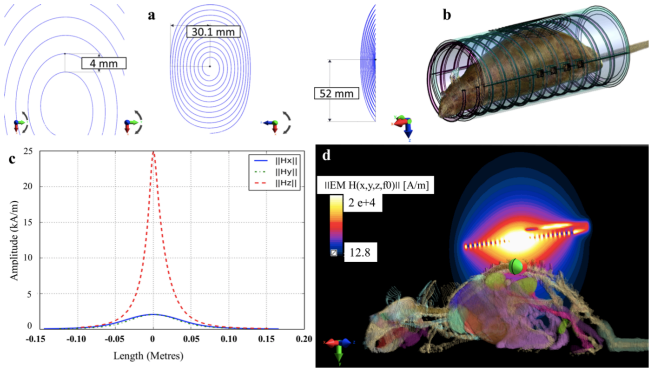

Figure 1. The curved planar coil setup for the *in vivo* experiments: the flux density numerical calculations regarding the setup for 56 Amps (RMS); (a) geometry of the curved planar coil (b) an anatomically correct 3D rat model exposed to AMF generated by the curved planar coil setup with a coil current of 56 Amps (RMS) together with the viewing window for thermal imaging, and the coil-shaped water jacket for maintaining physiological temperature can be seen in the *in vivo* coil setup - CAD model; (c) Magnetic field strength (H) along the main axis with regard to the coil middle; (d) Magnetic field strength XY-cross section passing through the middle of the coil (green ellipsoidal shape indicates the tumour position).

The physical evaluation of the prototype using a high-frequency magnetic field probe did correlate with the magnetic field calculations. Furthermore, as an example application, the magnetic field strength on the tumour surface was calculated as it is shown in Fig. 1d. This magnetic field can be considered as the effective one which leads to a further phenomenon like the eddy currents (see Fig. 2b), the magnetic power dissipation (see Fig. 2c) and finally to the temperature distribution within the tumour tissues (fig.2d). One should notice that the phenomenon mentioned above take place in the whole rat model and can be considered as the whole-body hyperthermia. Only the magnetic power losses can be controlled when magnetic nanoparticles are injected into the tumour in order to emphasise the temperature rise in the target area. In the case of presented setup, which was designed for *in vivo* experiments, it was able to heat a 5 mg /ml aqueous suspension of DMSA stabilized 10.3 nm sized magnetite nanoparticles by 3 - 5º C within 5 minutes, when a 2ml sample containing tube was placed in proximity to the centre of the coil. However, on the base of computer modelling, it was found that 5 mg/ml of magnetic nanoparticles concentration was too small to raise the temperature within the tumour.

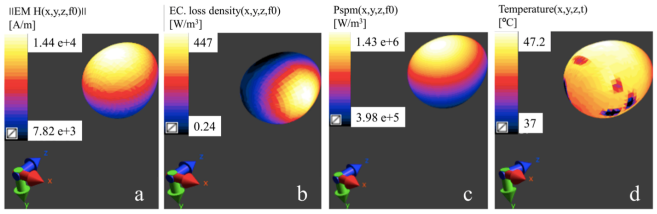

Figure 2. Numerical calculations are relative to the tumour from Fig. 1d: (a) Magnetic field strength on the tumour surface; (b) power density due to the eddy currents; (c) magnetic power loss density and (d) temperature distribution on the tumour surface after 1000 seconds of exposure.

That is why the concentration was increased to 15 mg/ml leading to magnetic power losses up to 1.4 MW/m^3, and the temperature rises to 47 ^{0}C in the tumour (see Fig. 2c-d). The following data were used in order to calculate the total magnetic power: the volume weighted log-normal distribution $g(\mu = 10.3, \sigma = 0.16, V_M)$, the magnetic saturation 92.0 kA/m, the anisotropy constant 30 kJ/m^3, the surfactant layer thickness 2.0 nm and density 5180 kg/m^3 which are equivalent to the physical properties of the magnetite. Moreover, the tumour tissue with MNPs was treated as a homogeneous composite. Even though the proposed design would be ideal for real-time full body thermal imaging while simultaneously maintaining physiological temperature within the animal chamber, the heating efficiency of the curved planar coil, and the homogeneity of the incident flux density was low when compared to the aforementioned 17 turn solenoid coil (11 º C within 5 minutes). Hence, further investigation of the coil design is required in order to improve its efficiency for such experiments. Though, the numerical calculations performed in this study will help researchers in planning *in-vivo* experiments using such anatomically correct female-rat models with tumours.

Fig. 2 shows the numerical calculations relative to the rat 3D model placed within the curved planar coil setup. Studies based on nanoparticles with equal saturation magnetisation but varying magnetic anisotropy, suggest that the latter parameter plays a crucial role in the transition from the linear to the non-linear regime when the flux density is increased. Calculations based on Linear Response Theory, the Stochastic Landau-Lifshitz method and kinetic Monte-Carlo

models have been used to understand the effect of material properties and inter-particle interactions on specific heat power. Such studies help us engineer magnetic fluids with better magneto-thermal properties for hyperthermia applications. However, discrepancies with estimated parameters and theoretical predictions arising due to particle-particle interactions need to be accounted for. Moreover, we need to acknowledge that accurate prediction of SAR is difficult [26-28].

IV. Conclusion

The instrumentation developed and described here, i.e. *in vivo* coil setup does require further development. Nevertheless, such *in silico* evaluations will provide knowledge to design suitable AMF applicators for AC magnetic field-mediated *in vivo* MNP heating as demonstrated in this study [29].

References

[1] M. Subramanian, A. Miaskowski, G. Pearce, J. Dobson, "A coil system for real-time magnetic fluid hyperthermia microscopy studies," *Int. J. Hyperthermia*, vol. 32, pp. 112-120, 2016.

[2] M. Subramanian, G. Pearce, O. K. Guldu, V. Tekin, A. Miaskowski, O. Aras, P. Unak, "A pilot study into the use of FDG-mNP as an alternative approach in neuroblastoma cell hyperthermia," *IEEE transactions on nanobioscience*, vol. 15, pp. 517-25, 2016.

[3] A. Skumiel, T. Hornowski, A. Józefczak, M. Koralewski, B. Leszczyński, "Uses and limitation of different thermometers for measuring heating efficiency of magnetic fluids," *Appl. Therm. Eng,* vol. 100, pp. 1308-1318, 2016.

[4] H. F. Rodrigues, F. M. Mello, L. C. Branquinho, N. Zufelato, E. P. Silveira-Lacerda, A. F. Bakuzis, "Real-time infrared thermography detection of magnetic nanoparticle hyperthermia in a murine model under a non-uniform field configuration," *Int. J. Hyperthermia,* vol. 29, pp. 752-67, 2013.

[5] L. C. Rose, J. C. Bear, P. Southern, P .D. McNaughter, R. B. Piggott, I. P. Parkin, S. Qi, B. P. Hills, A. G. Mayes, "On-demand, magnetic hyperthermia-triggered drug delivery: optimisation for the GI tract," *J. Mater. Chem. B,* vol. 4, pp. 1704-11, 2016.

[6] T. M. Elkhova, Y. K. Gun'ko, A. P. Pyatakov, Y. I. Spichkin, K. Dawson, A. M. Tishin, "The Expeimental Setup for Measuring of Thermal Parameters of Magnetic Fluids in AC Magnetic Field," *Solid. State. Phenom,* vol. 215, pp. 454-458, 2014.

[7] H. Rahn, S. Schenk, H. Engler, S. Odenbach, "Tissue model for the study of heat transition during magnetic heating treatment," *IEEE Trans. Magn,* vol. 49, pp. 244-249, 2013.

[8] S. L. Fossheim, K. A. Il'yasov, J. Hennig, A. Bjørnerud, "Thermosensitive paramagnetic liposomes for temperature control during MR imaging-guided hyperthermia: in vitro feasibility studies," *Academic radiology*, vol. 7, pp. 1107-15, 2000.

[9] S. Dutz, R. Hergt, "Magnetic nanoparticle heating and heat transfer on a microscale: basic principles, realities and physical limitations of hyperthermia for tumor therapy," *Int. J. of Hyperthermia*, vol. 29, pp. 790-800, 2013.

[10] A. Miaskowski, B. Sawicki, A. Krawczyk, "The use of magnetic nanoparticles in low frequency inductive hyperthermia," *COMPEL-The international journal for computation and mathematics in electrical and electronic engineering*, vol. 31, pp.1096-104, 2012.

[11] A. Miaskowski, B. Sawicki, M. Subramanian, "Identification of diffusion coefficients in heat equation on the base of non-adiabatic measurements of ferrofluids," in *2016 Proc. IEEE. Int. Conf. Computational Problems of Electrical Engineering (CPEE)* pp. 1-4.

[12] A. Miaskowski, M. Subramanian, "Specific absorption rate parameter model in magnetic hyperthermia," in *2017 Proc. IEEE. Int. Conf. Computational Problems of Electrical Engineering (CPEE)* pp. 1-4.

[13] A. Miaskowski, B. Sawicki, M. Subramanian, "Single-domain nanoparticle magnetic power losses calibrated with calorimetric measurements," *Bulletin of the Polish Academy of Sciences Technical Sciences*, pp. 1-8, 2018.

[14] H. H. Pennes, "Analysis of tissue and arterial blood temperatures in the resting human forearm," *J. Appl. Physiol,* vol. 1, pp. 93-122, 1948.

[15] P. A. Hasgall, F. Di Gennaro, C. Baumgartner, E. Neufeld, M. C. Gosselin, D. Payne, A. Klingenböck, N. Kuster, "IT'IS Database for thermal and electromagnetic parameters of biological tissues," Version 3.0. 10.13099/VIP21000-03-0, www.itis.ethz.ch/database, 2015.

[16] A. Christ, W. Kainz, E. G. Hahn, K. Honegger, M. Zefferer, E. Neufeld, W. Rascher, R. Janka, W. Bautz, J. Chen, B. Kiefer, "The Virtual Family—development of surface-based anatomical models of two adults and two children for dosimetric simulations. *Physics in medicine and biology*, vol. 55, pp. N23, 2009.

[17] S. Mannucci, L. Ghin, G. Conti, S. Tambalo, A. Lascialfari, T. Orlando, D. Benati, P. Bernardi, N. Betterle, R. Bassi, P. Marzola, "Magnetic nanoparticles from Magnetospirillum gryphiswaldense increase the efficacy of thermotherapy in a model of colon carcinoma," *PloS one*, vol. 9, pp. e108959, 2014.

[18] R. D. Corato, G. Béalle, J. Kolosnjaj-Tabi, A. Espinosa, O. Clément, A. K. A. Silva, C. Ménager and C. Wilhelm, "Combining magnetic hyperthermia and photodynamic therapy for tumor ablation with photoresponsive magnetic liposomes," *ACS Nano*, vol. 9, pp. 2904–16, 2015.

[19] A. Espinosa, R. D. Corato, J. Kolosnjaj-Tabi, P. Flaud, T. Pellegrino, C. Wilhelm, "Duality of iron oxide nanoparticles in cancer therapy: amplification of heating efficiency by magnetic hyperthermia and photothermal bimodal treatment," *ACS Nano*, vol. 10, pp. 2436–46, 2016.

[20] H. F. Rodrigues, G. Capistrano, F. M. Mello, N. Zufelato, E. Silveira-Lacerda, A. F. Bakuzis, "Precise determination of the heat delivery during in vivo magnetic nanoparticle hyperthermia with infrared thermography," *Physics in Medicine and Biology*, vol. 62, pp. 4062, 2017.

[21] B. B. Lahiri, S. Ranoo, J. Philip, "Infrared thermography based magnetic hyperthermia study in Fe 3 O 4 based magnetic fluids," *Infrared Physics & Technology*, vol. 78, pp. 173-84, 2016.

[22] C. L. Dennis, K. L. Krycka, J. A. Borchers, R. D. Desautels, J. Van Lierop, N. F. Huls, A. J. Jackson, C. Gruettner, R. Ivkov, "Internal magnetic structure of nanoparticles dominates time-dependent relaxation processes in a magnetic field," *Adv. Funct. Mater*, vol. 25, pp. 4300-4311, 2015.

[23] G. Vallejo-Fernandez, O. Whear, A. G. Roca, S. Hussain, J. Timmis, V. Patel, K. O'Grady, "Mechanisms of hyperthermia in magnetic nanoparticles," *J Phys D Appl Phys*, vol. 46, pp. 312001, 2013.

[24] M. Boskovic, G. F. Goya, S. Vranjes-Djuric, N. Jovic, B. Jancar, B. Antic, "Influence of size distribution and field amplitude on specific loss power," *J Appl Phys*, vol. 117, pp. 103903, 2015.

[25] L. C. Branquinho, M. S. Carrião, A. S. Costa, N. Zufelato, M. H. Sousa, R. Miotto, R. Ivkov, A. F. Bakuzis, "Effect of magnetic dipolar interactions on nanoparticle heating efficiency: Implications for cancer hyperthermia," *Scientific reports*, vol. 3, pp. 2887, 2013.

[26] E. L. Verde, G. T. Landi, M.S. Carrião, A. L. Drummond, J. A. Gomes, E. D. Vieira, M. H. Sousa, A. F. Bakuzis, "Field dependent transition to the non-linear regime in magnetic hyperthermia experiments: Comparison between maghemite, copper, zinc, nickel and cobalt ferrite nanoparticles of similar sizes," *Aip Advances*, vol. 2, pp. 032120, 2012.

[27] E. L. Verde, G. T. Landi, J. D. Gomes, M. H. Sousa, A. F. Bakuzis, "Magnetic hyperthermia investigation of cobalt ferrite nanoparticles: Comparison between experiment, linear response theory, and dynamic hysteresis simulations," *Journal of Applied Physics*, vol. 111, pp. 123902, 2012.

[28] S. Ruta, R. Chantrell, O. Hovorka, "Unified model of hyperthermia via hysteresis heating in systems of interacting magnetic nanoparticles," *Scientific reports*, vol. 5, pp. 9090, 2015.

[29] M. Subramanian, A. Miaskowski, A. K. Mahapatro, J. Dobson, "Practical bioinstrumentation developments for AC magnetic field-mediated magnetic nanoparticle heating applications," *Applied Physics A*, vol. 3, pp. 194, 2019.